

PROCEEDINGS OF SPIE

[SPIDigitalLibrary.org/conference-proceedings-of-spie](https://spiedigitallibrary.org/conference-proceedings-of-spie)

High efficiency planar geometry germanium-on-silicon single-photon avalanche diode detectors

Thorburn, Fiona, Huddleston, Laura, Kirdoda, Jarosław, Millar, Ross, Ferre-Llin, Lourdes, et al.

Fiona E. Thorburn, Laura L. Huddleston, Jarosław Kirdoda, Ross W. Millar, Lourdes Ferre-Llin, Xin Yi, Douglas J. Paul, Gerald S. Buller, "High efficiency planar geometry germanium-on-silicon single-photon avalanche diode detectors," Proc. SPIE 11386, Advanced Photon Counting Techniques XIV, 113860N (18 May 2020); doi: 10.1117/12.2559620

SPIE.

Event: SPIE Defense + Commercial Sensing, 2020, Online Only, California, United States

High Efficiency, Planar Geometry Germanium-on-Silicon Single-Photon Avalanche Diode Detectors

Fiona E. Thorburn^a, Laura L. Huddleston^a, Jarosław Kirdoda^b, Ross W. Millar^b,
 Lourdes Ferre-Llin^b, Xin Yi^a, Douglas J. Paul^b, Gerald S. Buller^{*a}

^aInstitute of Photonics and Quantum Sciences, School of Engineering and Physical Sciences, Heriot-Watt University, Edinburgh, EH14 4AS, United Kingdom;

^bJames Watt School of Engineering, University of Glasgow, Rankine Building, Oakfield Avenue, Glasgow, G12 8LT, United Kingdom

ABSTRACT

This paper presents the performance of 26 μm and 50 μm diameter planar Ge-on-Si single-photon avalanche diode (SPAD) detectors. The addition of germanium in these detectors extends the spectral range into the short-wave infrared (SWIR) region, beyond the capability of already well-established Si SPAD devices. There are several advantages for extending the spectral range into the SWIR region including: reduced eye-safety laser threshold, greater attainable ranges, and increased depth resolution in range finding applications, in addition to the enhanced capability to image through obscurants such as fog and smoke. The time correlated single-photon counting (TCSPC) technique has been utilized to observe record low dark count rates, below 100 kHz at a temperature of 125 K for up to a 6.6 % excess bias, for the 26 μm diameter devices. Under identical experimental conditions, in terms of excess bias and temperature, the 50 μm diameter device consistently demonstrates dark count rates a factor of 4 times greater than 26 μm diameter devices, indicating that the dark count rate is proportional to the device volume. Single-photon detection efficiencies of up to $\sim 29\%$ were measured at a wavelength of 1310 nm at 125 K. Noise equivalent powers (NEP) down to $9.8 \times 10^{-17} \text{ WHz}^{-1/2}$ and jitters $< 160 \text{ ps}$ are obtainable, both significantly lower than previous 100 μm diameter planar geometry devices, demonstrating the potential of these devices for highly sensitive and high-speed imaging in the SWIR.

Keywords: Single-photon, Lidar, Avalanche photodiodes, Photodetectors

1. INTRODUCTION

Devices which are capable of the detection of single-photons using impact ionization in avalanche diodes have become vital for in several emerging applications areas. These applications include Light Detection and Ranging (LiDAR) and 3D imaging using time-of-flight¹⁻³ or range-gating⁴, quantum key distribution (QKD)⁵, fiber/free space quantum communications^{6,7} and quantum optics⁸. CMOS based single-photon avalanche diode (SPAD) detectors have been commercially available for a number of years and are well-established as highly-sensitive, large area detector arrays with integrated electronics^{9,10}. The drawback of these devices, however, is that they are limited to operation below wavelengths of $\lambda \sim 1 \mu\text{m}$ because of the wide bandgap of Si. There are many advantages for extending the operating range of such devices beyond this limit and into the short-wave infrared (SWIR) spectral region. The ability to operate at the low-loss optical fiber telecommunications wavelengths of 1310 nm and 1550 nm is clearly essential for quantum communications applications which require high-speed and ultra-sensitive SWIR SPAD detectors. Free space applications, such as LiDAR, can also benefit greatly from operating in the SWIR because the eye-safety laser threshold increases substantially in this spectral range compared to wavelengths $< 1 \mu\text{m}$, thus much higher power optical sources can be utilized in active imaging resulting in improved depth resolution and longer obtainable maximum range¹¹. In addition to this, solar radiation which considerably increases the background level in many SPAD based LiDAR applications is significantly reduced in the SWIR¹². Finally, atmospheric transmission is greatly improved particularly when imaging through obscurants including, for example: smoke, dust, haze and snow, due to decreased Mie scattering in the SWIR spectral region^{13,14}. In the SWIR spectral region, the two most commonly used single-photon detectors are InGaAs/InP based SPADs and superconducting nanowire detectors. The latter provide particularly high performance for single-photon detection [15],

*g.s.buller@hw.ac.uk; single-photon.com

however, their practicality is limited for some applications due to cryogenic cooling requirements, as they are typically operated at temperatures less than 3 K. InGaAs/InP SPADs have been extensively developed to the point that high-performance imaging array cameras have been developed and demonstrated in several single-photon depth imaging applications^{3,15-17}. Typically, InGaAs/InP based SPADs exhibit single-photon detection efficiencies (SPDEs) ranging from 20 % to > 50 % in the SWIR and operate at Peltier-cooled temperatures between 220 K and 255 K¹⁸⁻²³, this is advantageous because Peltier-cooling has less stringent requirements for size, weight and power consumption in comparison to cryogenic cooling, facilitating the development of compact detector modules. Another challenge associated with InGaAs based SPADs is that the achievable count rates are markedly restricted by prominent afterpulsing effects²⁴⁻²⁶, however, progress continues to be made in mitigating this issue^{21,27}.

An alternative to these methods is to use germanium as an absorber; the bandgap of Ge allows for efficient photon absorption at wavelengths up to ~ 1600 nm at room temperature. Dual temperature growth techniques have resulted in high quality Ge layers grown on Si²⁸, facilitating the fabrication of optical detectors capable of absorption potentially up to $\lambda \sim 1600$ nm and the potential to be fabricated in Si foundries. Effective and reliable fabrication techniques have made possible many demonstrations of Ge-on-Si PIN diodes and linear avalanche photodetectors with impressive performance²⁸⁻³⁰. The first single-photon detector using a Ge-containing absorber adjacent to a Si multiplication layer was reported in 2002 by Loudon et al. in which they utilized a SiGe/Si multiple quantum well structure to absorb 1210 nm wavelength photons³¹. In 2011 Lu et al. presented a Ge-on-Si SPAD with SPDE up to 14 % and dark count rates (DCRs) of the order of 100s of Mcps (counts per second) at a temperature of 200 K, for a wavelength of 1310 nm³². Shortly after, Warburton et al. reported a mesa etched design which at the same wavelength obtained an SPDE of 4 % and DCR of 6 Mcps at 100 K²⁴, and also for the first time demonstrated single-photon detection at 1550 nm from a Si based device. The disadvantage of the mesa geometry associated with the SPADs reported in^{24,32}, is that the exposed sidewalls of the devices contribute significantly to the DCR, resulting in high values of the order of Mcps, which places serious restrictions on the device performance. Martinez et al. demonstrated a solution to this in 2017 through the use of a waveguide coupled Ge-on-Si SPAD at 80 K, which exhibited an SPDE of 5.27 % and much improved DCR of 534 kcps at a wavelength of 1310 nm³³. Another alternative design which avoids the limitations imposed by the exposed sidewalls is that of a planar geometry design ensuring that the high field region is maintained far from any sidewall. We previously reported a planar device with an active area diameter of 100 μm exhibiting an impressive SPDE of 38 % at 1310 nm for a temperature of 125K. Due to a relatively large diameter, however, the device exhibited a rather high DCR of 2 Mcps²⁵. A planar geometry 100 μm diameter Ge-on-Si SPAD was subsequently utilized for laboratory-based-LiDAR experiments at short ranges which allowed modelling of performance under more realistic scenarios of operation³⁴, clearly demonstrating the potential of these devices in 3D imaging applications.

In this paper, we report on the performance of 26 μm and 50 μm diameter planar Ge-on-Si SPADs and compare the results to prior planar devices. A significant reduction in the DCR is observed with these smaller area devices and we conclude that the DCR scales proportionally with volume. SPDEs up to ~ 29 % are demonstrated at 125 K for a wavelength of 1310 nm, although less than the 38 % reported for a larger 100 μm diameter device²⁵, it is proposed that this is limited by experimental design rather than the device itself. The particularly low DCR displayed by the 26 μm diameter detector indicates a highly sensitive single-photon detector, quantified by a noise equivalent power (NEP) of 9.8×10^{-17} $\text{WHz}^{-1/2}$; seven times lower than that observed from the 100 μm diameter planar geometry devices, at the same temperature. Furthermore, low jitter performance is demonstrated; down to 157 ± 10 ps.

2. EXPERIMENTAL PROCEDURE

2.1 Device fabrication

The SPADs were grown on 150 mm diameter n^{++} -Si (001) substrates. First, a 1.5 μm thickness of nominally undoped Si was grown epitaxially using a commercial reduced pressure chemical vapor deposition (RPCVD) system. Subsequently, photolithography was used to define windows for the charge sheet layers for each SPAD device. The doping level and thickness of the charge sheet layer controls the relative electric field profiles in the Ge absorber and Si avalanche region. The devices were implanted using boron at 10 keV and activated with a 30s anneal at 950°C. The wafers were cleaned,

then 1 μm of undoped Ge was grown before a 50 nm $\text{p}^{++}\text{-Ge}$ cap which constitutes the top contact. The $\text{p}^{++}\text{-Ge}$ top contact area was etched using photolithography and a fluorine inductively coupled plasma reactive ion etch (ICP-RIE). Photolithography was also used to define trenches between the SPAD devices and a fluorine ICP-RIE etched through the Ge epilayers to provide lateral electrical isolation. The device was planarized with hydrogen silsesquioxane (HSQ) and plasma enhanced chemical vapor deposition (PECVD) SiO_2 . Next, Ti/Al was evaporated onto the backside of the wafers and annealed to form a bottom Ohmic contact to the $\text{n}^{++}\text{-Si}$ substrate followed by photolithography again to form holes to the p^{++} cap, then Ti/Al was deposited to form an Ohmic contact to the top of the device. Lastly, a silicon nitride anti-reflection coating was deposited by PECVD on top of the device to reduce surface reflections. A detailed description of the whole process can be found in ²⁵. A cross-section of a single planar geometry Ge-on-Si SPAD is shown in Figure 1(a) and a microscope image of the top view of a chip containing planar Ge-on-Si SPADs is shown in Figure 1(b).

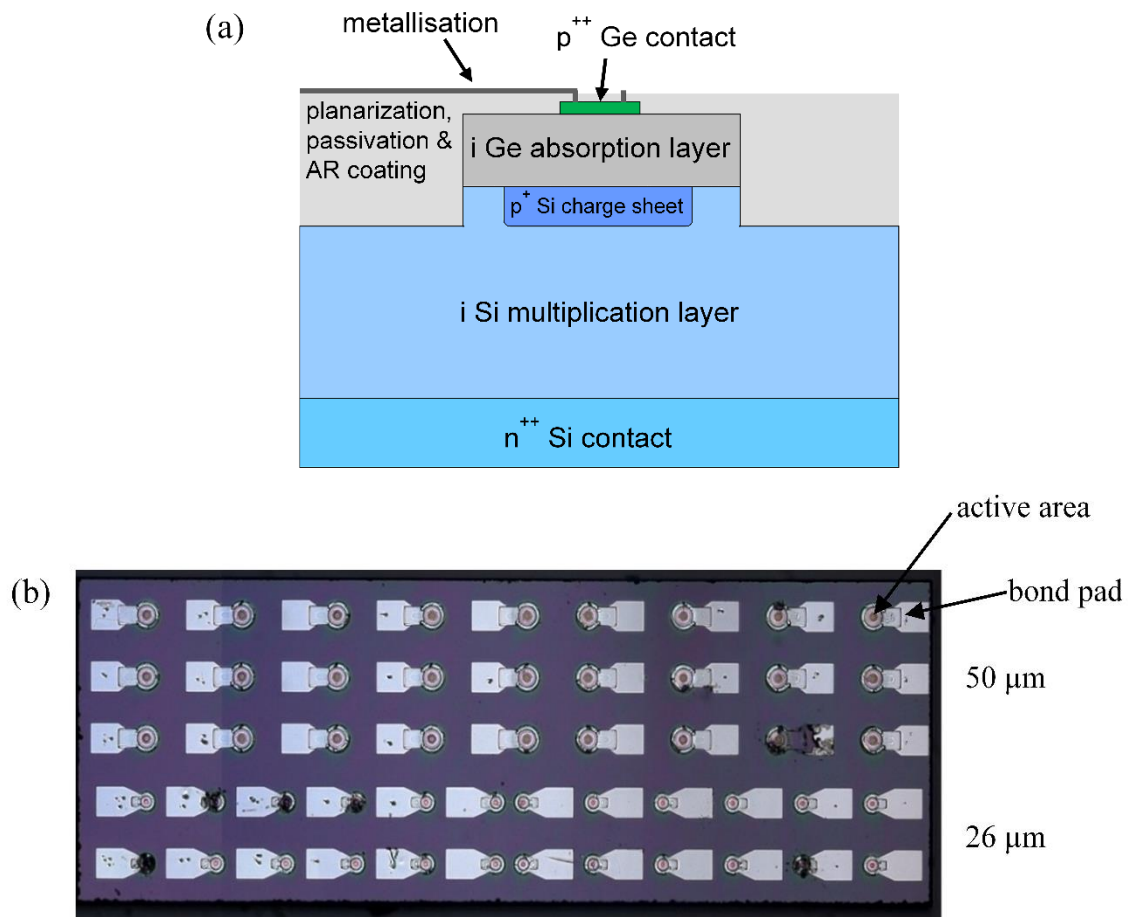


Figure 1. (a) A cross-section of a planar Ge-on-Si SPAD. This diagram shows the silicon bottom contact, multiplication and charge sheet layers, as well as the germanium absorption and top contact layers and finally, the planarization, passivation, AR coating and metallization layers (i = intrinsic). (b) A microscope image at $\times 5$ magnification of a chip containing three rows of $50\ \mu\text{m}$ diameter and 2 rows of $26\ \mu\text{m}$ diameter Ge-on-Si SPADs, the metal bond pad and device active area are highlighted.

2.2 Detector characterization using time-correlated single-photon counting (TCSPC)

A schematic diagram of the experimental set-up used to measure the SPDE, DCR and jitter parameters is shown in Figure 2.

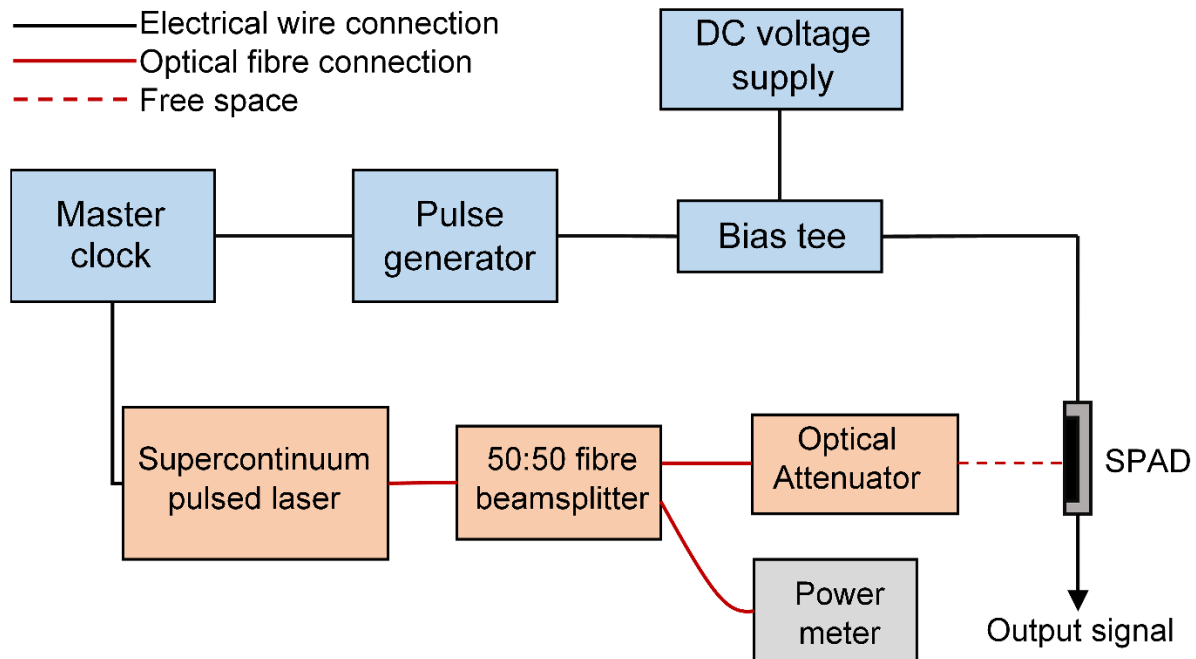


Figure 2. A schematic diagram of the TCSPC experimental set-up. The SPAD was mounted in a variable temperature cryostat on a translation stage with 3D movement. The optical alignment of the focused attenuated beam onto the detector active area was performed using an illuminated SWIR camera arrangement (not shown in the diagram).

The chip containing the SPADs was mounted in a variable temperature Oxford Instruments cryostat which was maintained at a temperature of 125 K for these measurements. The laser used was a pulsed NKT Supercontinuum laser, tunable in the wavelength range of 1150 – 2000 nm. The laser's output was coupled into a single mode optical fiber and directed into an in-fiber 50:50 beam splitter. One output from the splitter was measured by a calibrated power meter to allow continuous monitoring of the power level to the optical system. The other output was directed to through a calibrated optical attenuator with a maximum attenuation of 100 dB, and then a lens focused the output from this onto the device active area. A second, removable, power meter was utilized to measure the power after the lens and thus calculate the attenuation required to result in less than 0.01 photons per pulse incident upon the SPAD, ensuring the probability of > 1 photon per pulse was statistically negligible. A fixed direct current (DC) voltage at a level just below the avalanche breakdown voltage was applied to the device under investigation and a gated voltage supplied by the pulse generator was applied to periodically take the device above the avalanche breakdown level for a gate of ~ 50 ns. This gated signal was applied in synchronization with the incident optical attenuated pulses from the laser, allowing the SPAD to operate in the Geiger mode whilst the photons are incident. Outside of the gating pulses, the detector was held below avalanche breakdown until the next optical pulse was incident. The cathode of the SPAD was connected to the photon counting data acquisition unit and the measurements were taken at a low repetition rate of 10 kHz to minimize the probability of afterpulsing affecting the measurements.

3. RESULTS

The SPDE and DCR for both the 26 μm and 50 μm diameter devices are displayed in Figures 3(a) and (b) respectively as a function of excess bias.

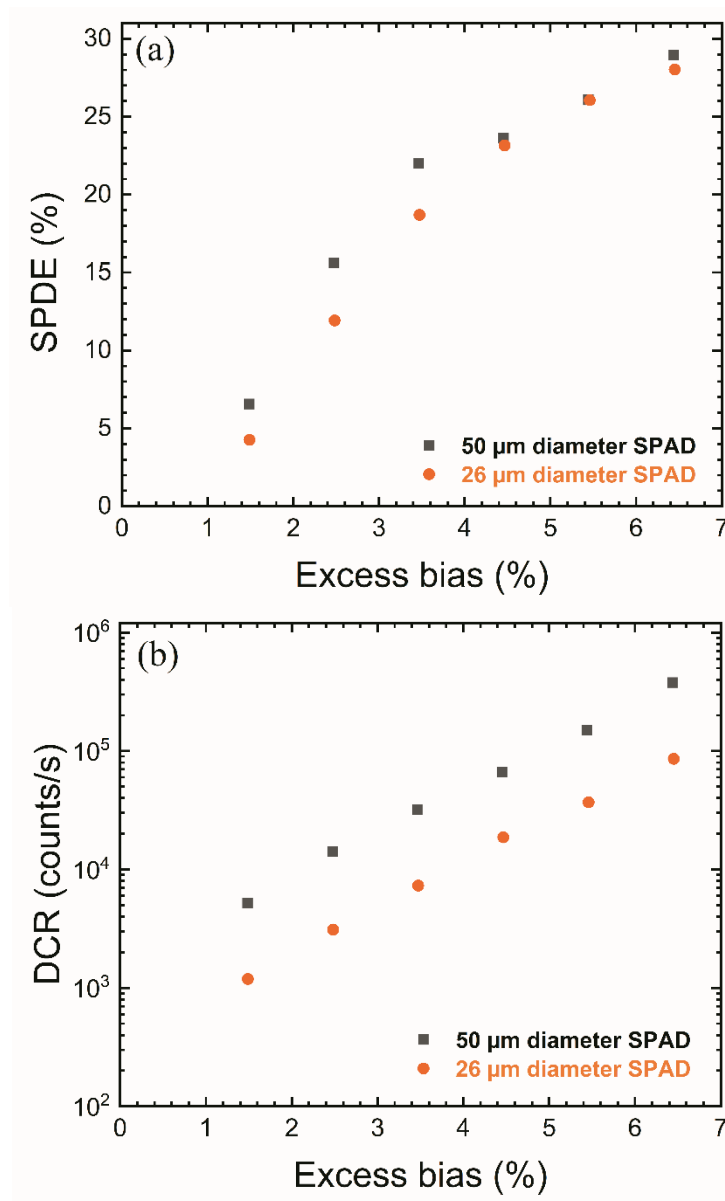


Figure 3. (a) The SPDE and (b) DCR of the 26 μm and 50 μm diameter Ge-on-Si SPADs as a function of excess bias at a temperature of 125 K. The SPDE values were measured at an incident photon wavelength of 1310 nm.

As can be observed in Figure 3(a), the maximum SPDEs measured were 28 % and 29 % for the 26 μm and 50 μm diameter devices respectively, at a 6.5 % excess bias. This is 10 % lower than that of the 100 μm device reported previously, it is proposed that this may be partly because the 26 μm and 50 μm diameter devices at present may not collect all photons during the SPDE measurements. Further work is needed in order to identify any other mechanisms which may account for the decrease in SPDE for these smaller area devices. In Figure 3(b), it can be seen that the DCR for the 26 μm device remains below 100 kcps for excess bias up to the maximum of 6.5 %. The DCR for the larger 50 μm device is consistently ~ 4 times greater than for the smaller device, reaching a maximum of ~ 380 kcps for an excess bias of 6.5 %. This is 4.4 times greater than the DCR for the 26 μm device at the same bias, which measured ~ 86 kcps. These results suggest that the DCR is proportional to the device volume, indicating that surface contributions to the total DCR are minimal. With

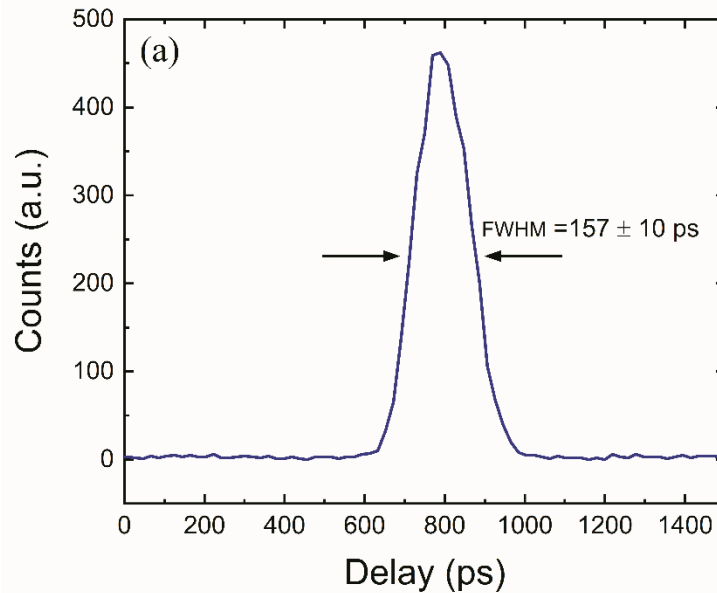
reference to our previous work²⁵, under the same experimental conditions in terms of wavelength and temperature, the DCRs reported for the 100 μm diameter planar device vary between 13.5 and 51 times greater than the 50 μm DCR levels reported here, up to an excess bias of 5.5 %. Although it may be expected that the DCR for the 100 μm diameter device should again be 4 times greater for twice the diameter, the former device was fabricated much earlier and the fabrication processes were significantly improved since, thus this has led to much improved DCR levels.

The NEP is a useful parameter for indicating the sensitivity of a SPAD detector and it is calculated from the SPDE and DCR using equation (1)

$$NEP = \frac{h\nu}{SPDE} \sqrt{2DCR} \quad (1)$$

where h represents Planck's constant and ν is the frequency of the incident photons. The NEP is useful for comparing detectors, with lower values indicating higher optical sensitivity. For the 26 μm diameter device, the minimum NEP was calculated as $9.8 \times 10^{-17} \text{ WHZ}^{-1/2}$ at an excess bias of ~ 3.5 % and for the 50 μm device the lowest NEP calculated was $1.6 \times 10^{-16} \text{ WHZ}^{-1/2}$ recorded at an excess bias of ~ 2.5 %. These figures represent a 7 and 4 fold reduction in this parameter respectively compared to the 100 μm diameter SPAD in²⁵. Whilst not as low as that of InGaAs/InP SPADs which have demonstrated NEP values down to $1 \times 10^{-17} \text{ WHZ}^{-1/2}$ for $\lambda = 1550 \text{ nm}$ at 223 K, these devices have shown considerable improvement compared to mesa geometry and larger area planar Ge-on-Si SPADs. Thus, work is ongoing to improve these devices by reducing the DCR to allow operation at higher temperatures consistent with Peltier-cooling.

The jitter of each device was measured as a function of excess bias and is expressed as the full-width-at-half-maximum of the timing histogram recorded in each case. The minimum jitter measured was $157 \pm 10 \text{ ps}$, this was recorded for the 26 μm diameter device at an excess bias of 6.5 % and the timing histogram is displayed in Figure 4 (a). Figure 4 (b) shows the jitter measured for both the 26 μm and 50 μm diameter devices as a function of the excess bias, as expected the jitter decreases with increasing excess bias. The 50 μm diameter device exhibited a minimum jitter of ~ $210 \pm 10 \text{ ps}$ for an excess bias of 6.5 %. The jitter reported for the 100 μm diameter planar SPAD in²⁵ was 310 ps for an excess bias of 5.5 %, measured at a lower temperature of 78 K. Therefore, the smaller area detectors improve the speed capability of the device as seen in other material systems, as a result of the restricted lateral extent of the avalanche build-up³⁵.



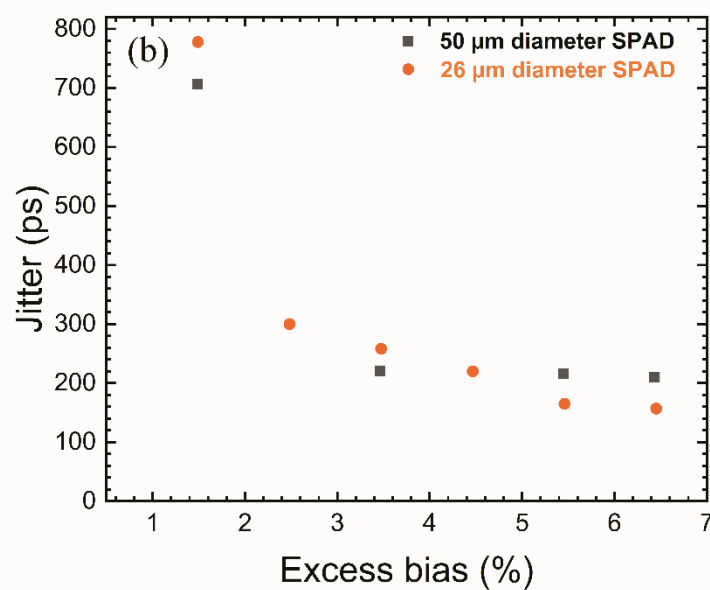


Figure 4. (a) Timing histogram for the minimum jitter recorded, this was obtained by the 26 μm diameter device at an excess bias of 6.5 %. (b) Temporal jitter, expressed as full-width-at-half-maximum, of the 26 μm and 50 μm diameter Ge-on-Si SPADs as a function of excess bias at a temperature 125 K for an incident wavelength of 1310 nm.

4. CONCLUSIONS

In summary, the performance of 26 μm and 50 μm diameter planar geometry Ge-on-Si SPADs has been investigated. At a wavelength of 1310 nm and temperature of 125 K, the 26 μm and 50 μm diameter SPADs exhibited maximum SPDE values of 28 % and 29 % respectively. The DCR observed from the 26 μm device was extremely low; staying below 100 kcps for an excess bias up to 6.5 %. The 50 μm diameter device DCR was approximately 4 times greater than 26 μm device at each excess bias level recorded and so proportional to the device volume. This preliminary result indicates that surface contributions to the overall DCR are minimal, an important result to help our understanding of the devices and developing the design and fabrication processes going forward. High-speed operation was also observed; the smaller diameter device exhibited the best performance with jitter down to 157 ± 10 ps, the results conclusively show that smaller devices reduce the device jitter as previously seen in SPADs fabricated in other material systems. Furthermore, high-sensitivity operation was also observed, this is quantified by a minimum NEP value of 9.8×10^{-17} $\text{WHz}^{-1/2}$ for the 26 μm diameter device representing a 7 fold reduction compared to a larger 100 μm diameter planar Ge-on-Si SPAD under similar experimental conditions. The results presented show that utilizing smaller diameter devices significantly improves the performance of Ge-on-Si Geiger mode detectors demonstrating the potential for highly efficient, fast and affordable single-photon detectors in the SWIR for a variety of applications.

ACKNOWLEDGEMENTS

The authors acknowledge the support of UK Engineering and Physical Sciences Research Council (EPSRC) projects UK EPSRC (EP/N003446/1, EP/L024020/1, EP/N003225/1, EP/S026428/1, EP/T00097X/1, EP/T001011/1); InnovateUK (104615); UK Royal Academy of Engineering Research Fellowship Scheme (Project RF-201819-18-187).

REFERENCES

- [1] Pawlikowska, A. M., Halimi, A., Lamb, R. A. & Buller, G. S., "Single-photon three-dimensional imaging at up to 10 kilometers range," *Opt. Express* 25(10), 11919-11931 (2017).

- [2] Tobin, R., Halimi, A., McCarthy, A., Ren, X., McEwan, K., McLaughlin, S. and Buller, G. S., "Long-range depth profiling of camouflaged targets using single-photon detection," *Optical Engineering* 57(3), 031303 (2017).
- [3] Tachella, J., Altmann, Y., Mellado, N., McCarthy, A., Tobin, R., Buller, G. S., Tourneret, J. and McLaughlin, S., "Real-time 3D reconstruction from single-photon lidar data using plug-and-play point cloud denoisers," *Nat. Commun.* 10, 4984 (2019).
- [4] Ren, X., Connolly, P. W. R., Halimi, A., Altmann, Y., McLaughlin, S., Gyongy, I., Henderson, R. K. and Buller, G. S., "High-resolution depth profiling using a range-gated CMOS SPAD quanta image sensor," *Opt. Express* 26(5), 5541-5557 (2018).
- [5] Takesue, H., Nam, S. W., Zhang, Q., Hadfield, R. H., Honjo, T., Tamaki, K. and Yamamoto, Y., "Quantum key distribution over a 40-dB channel loss using superconducting single-photon detectors," *Nat. Photonics* 1, 343-348 (2007).
- [6] Gordon, K. J., Fernandez, V., Townsend, P. D. and Buller, G. S., "A short wavelength GigaHertz clocked fiber-optic quantum key distribution system," *IEEE J. Quantum Electron.* 40(7), 900-908 (2004).
- [7] Pugh, C. J., Kaiser, S., Bourgoin, J., Jin, J., Sultana, N., Agne, S., Anisimova, E., Makarov, V., Choi, E. and Higgins, B. L., "Airborne demonstration of a quantum key distribution receiver payload," *Quantum Sci. Technol.* 2(2), 024009 (2017).
- [8] Tanzilli, S., Martin, A., Kaiser, F., De Micheli, M. P., Alibart, O. and Ostrowsky, D. B., "On the genesis and evolution of Integrated Quantum Optics," *Laser Photonics Rev.* 6(1), 115-143 (2012).
- [9] Rech, I., Gulinatti, A., Zappa, F., Ghiono, M and Cova, S., "High-performance silicon single-photon avalanche diode array," *Proc. SPIE* 7320, 73200H (2009).
- [10] Gyongy, I., Calder, N., Davies, A., Dutton, N. A. W., Duncan, R. R., Rickman, C., Dalgarno, P. and Henderson, R. K., "A 256 x 256 , 100-klfps, 61% Fill-Factor SPAD Image Sensor for Time-Resolved Microscopy Applications," *IEEE Trans. Electron Devices* 65(2), 547-554 (2018).
- [11] Wallace, A. M., Halimi, A. and Buller, G. S., "Full waveform LiDAR for adverse weather conditions," *IEEE Trans. Veh. Technol.*, doi:10.1109/TVT.2020.2989148 (2020).
- [12] Bird, R. E., Hulstrom, R. L. and Lewis, L. J., "Terrestrial solar spectral data sets," *Solar Energy* 30(6), 563-573 (1983).
- [13] Arnulf, A., Bricard, J., Curé, E. and Véret, C., "Transmission by Haze and Fog in the Spectral Region 0.35 to 10 Microns*," *J. Opt. Soc. Am.* 47(6), 491-498 (1957).
- [14] Tobin, R., Halimi, A., McCarthy, A., Laurenzis, M., Christnacher, F. and Buller, G. S., "Three-dimensional single-photon imaging through obscurants," *Opt. Express* 27(4), 4590-4611 (2019).
- [15] Itzler, M. A., Entwistle, M., Owens, M., Patel, K., Jiang, X., Slomkowski, K., Rangwala, S., Zalud, P. F., Senko, T., Tower, J. and Ferraro, J., "Comparison of 32 x 128 and 32 x 32 Geiger-mode APD FPAs for single photon 3D LADAR imaging" *Proc. SPIE* 8033, 80330G (2011).
- [16] Laurenzis, M., "Single photon range, intensity and photon flux imaging with kilohertz frame rate and high dynamic range," *Opt. Express* 27(26), 38391-38403 (2019).
- [17] Legros, Q., Tachella, J., Tobin, R., McCarthy, A., Meignen, S., Buller, G. S., Altmann, Y., McLaughlin, S. and Davies, M. E., "Robust 3D reconstruction of dynamic scenes from single-photon lidar using Beta-divergences," arXiv:2004.09211 (2020).
- [18] Pellegrini, S., Warburton, R. E., Tan, L. J. J., Ng, J. S., Krysa, A. B., Groom, K., David, J. P. R., Cova, S., Robertson, M. J. and Buller, G. S., "Design and performance of an InGaAs-InP single-photon avalanche diode detector," *IEEE J. Quantum Electron.* 42(4), 397-403 (2006).
- [19] Campbell, J. C., Sun, W., Lu, Z., Itzler, M. A. and Jiang, X., "Common-Mode Cancellation in Sinusoidal Gating With Balanced InGaAs/InP Single Photon Avalanche Diodes," *IEEE J. Quantum Electron.* 48(12), 1505-1511 (2012).
- [20] Tosi, A., Calandri, N., Sanzaro, M. and Acerbi, F., "Low-Noise, Low-Jitter, High Detection Efficiency InGaAs/InP Single-Photon Avalanche Diode," *IEEE J. Sel. Topics Quantum Electron.* 20(6), 192-197 (2014).
- [21] Zhang, J., Itzler, M. A., Zbinden, H. & Pan, J.-W., "Advances in InGaAs/InP single-photon detector systems for quantum communication," *Light Sci. Appl.* 4, e286 (2015).
- [22] Comandar, L. C., Fröhlich, B., Dynes, J. F., Sharpe, A. W., Lucamarini, M., Yuan, Z. L., Pentz, R. V. and Shields, A. J., "Gigahertz-gated InGaAs/InP single-photon detector with detection efficiency exceeding 55% at 1550 nm," *J. Appl. Phys.* 117(8), 083109 (2015).
- [23] Restelli, A., Bienfang, J. C. and Migdall, A. L., "Single-photon detection efficiency up to 50% at 1310 nm with an InGaAs/InP avalanche diode gated at 1.25 GHz," *Appl. Phys. Lett.* 102(14), 141104 (2013).

- [24] Warburton, R. E., Intermite, G., Myronov, M., Allred, P., Leadley, D. R., Gallacher, K., Paul, D. J., Pilgrim, N. J., Lever, L. J. M., Ikonic, Z., Kelsall, R. W., Huante-Cerón, E., Knights, A. P. and Buller, G. S., “Ge-on-Si Single-Photon Avalanche Diode Detectors: Design, Modeling, Fabrication, and Characterization at Wavelengths 1310 and 1550 nm,” *IEEE Trans. Electron Devices* 60(11), 3807-3813 (2013).
- [25] Vines, P., Kuzmenko, K., Kirdoda, J., Dumas, D. C. S., Mirza, M. M., Millar, R. W., Paul, D. J. and Buller, G. S., “High performance planar germanium-on-silicon single-photon avalanche diode detectors,” *Nat. Commun.* 10, 1086 (2019).
- [26] Itzler, M. A., Jiang, X., Entwistle, M., Slomkowski, K., Tosi, A., Acerbi, F., Zappa, F. and Cova, S., “Advances in InGaAsP-based avalanche diode single photon detectors,” *J. Mod. Opt.* 58(3-4), 174-200 (2011).
- [27] Scarcella, C., Boso, G., Ruggeri, A. and Tosi, A., “InGaAs/InP Single-Photon Detector Gated at 1.3 GHz With 1.5% Afterpulsing,” *IEEE J. Sel. Topics Quantum Electron.* 21(3), 17-22 (2015).
- [28] Michel, J., Liu, J. and Kimerling, L. C., “High-performance Ge-on-Si photodetectors,” *Nat. Photonics* 4, 527-534 (2010).
- [29] Huang, M., Li, S., Cai, P., Hou, G., Su, T., Chen, W., Hong, C. and Pan, D., “Germanium on Silicon Avalanche Photodiode,” *IEEE J. Sel. Topics Quantum Electron.* 24(2), 1-11 (2018).
- [30] Virot, L., Crozat, P., Fédéli, J.-M., Hartmann, J.-M., Marris-Morini, D., Cassan, E., Boeuf, F. and Vivien, L., “Germanium avalanche receiver for low power interconnects,” *Nat. Commun.* 5, 4957 (2014).
- [31] Loudon, A. Y., Hiskett, P. A., Buller, G. S., Carline, R. T., Herbert, D. C., Leong, W. Y. and Rarity, J. G., “Enhancement of the infrared detection efficiency of silicon photon-counting avalanche photodiodes by use of silicon germanium absorbing layers,” *Opt. Lett.* 27(4), 219-221 (2002).
- [32] Lu, Z., Kang, Y., Hu, C., Zhou, Q., Liu, H.-D. and Campbell, J. C., “Geiger-Mode Operation of Ge-on-Si Avalanche Photodiodes,” *IEEE J. Quantum Electron.* 47(5), 731-735 (2011).
- [33] Martinez, N. J. D., Gehl, M., Derose, C. T., Starbuck, A. L., Pomerene, A. T., Lentine, A. L., Trotter, D. C. and Davids, P. S., “Single photon detection in a waveguide-coupled Ge-on-Si lateral avalanche photodiode,” *Opt. Express* 25(14), 16130-16139 (2017).
- [34] Kuzmenko, K., Vines, P., Halimi, A., Collins, R. J., Maccarone, A., McCarthy, A., Greener, Z. M., Kirdoda, J., Dumas, D. C. S., Llin, L. F., Mirza, M. M., Millar, R. W., Paul, D. J., Buller, G. S., “3D LIDAR imaging using Ge-on-Si single photon avalanche diode detectors,” *Opt. Express* 28(2), 1330-1344 (2020).
- [35] Lacaita, A., Spinelli, A. and Longhi, S., “Avalanche transients in shallow p-n junctions biased above breakdown,” *Appl. Phys. Lett.* 67(18), 2627-2629 (1995).